Aerosol and Air Quality Research, 12: 707–721, 2012

ISSN: 1680-8584 print / 2071-1409 online
doi: 10.4209/aaqr.2011.11.0225

Modeling the Regional Dynamics of Gaseous Admixtures and Aerosols in the Areas of Lake Baikal (Russia) and Antwerp (Belgium)

A.E. Aloyan[1], V.O. Arutyunyan[1], A.N. Yermakov[2], V.A. Zagaynov[3], C. Mensink[4*], K. De Ridder[4], K. Van de Vel[4], F. Deutsch[4]

[1] *Institute of Numerical Mathematics, Russian Academy of Sciences, Russia*
[2] *Institute of Energy Problems of Chemical Physics, Russian Academy of Sciences, Moscow, Russia*
[3] *Karpov Institute of Physical Chemistry, Moscow, Russia*
[4] *Flemish Institute for Technological Research (VITO), Mol, Belgium*

ABSTRACT

A combined mathematical model was developed for the regional-scale dynamics of gaseous admixtures and aerosols in the atmosphere. The model incorporates the following modules: thermo-hydrodynamic equations for meso-scale atmospheric processes in the non-hydrostatic approximation; transport of gaseous admixtures and aerosols, with allowance for photochemical transformation and binary homogeneous nucleation; and kinetic processes of condensation/evaporation and coagulation. Particular emphasis is given to the mechanisms of new-particle formation through binary homogeneous nucleation of drops of sulfuric acid and water vapor. By using this model, numerical experiments were performed to investigate spatio-temporal variations in the concentrations of gaseous admixtures and aerosols, as well as the formation of fine aerosol clusters in the Lake Baikal (Russia) and Antwerp (Belgium) areas due to strong industrial emission sources. The results of the numerical experiments are analyzed.

Keywords: Air pollution; Particulate matter; Regional air quality; Dispersion modeling.

INTRODUCTION

The atmosphere is known to contain emissions of many gas- and aerosol-phase chemical substances emitted from the Earth's surface. In the atmosphere, these substances undergo a series of chemical and physical transformations through atmospheric circulation, photochemistry, homogeneous nucleation, condensation/evaporation, and coagulation. Since all these processes are interconnected, there is good reason to consider them within the framework of a single model.

The objective of this paper is to develop a regional aerosol model which describes these interacting physical and chemical processes in a correct way using state of the art numerical solution techniques. A further objective is to make the model generic and show that it can be used and applied for regional scale assessments in geographically different regions.

With these objectives in mind the model was applied in two different study areas: Lake Baikal in Russia on one hand and the densely populated industrialized area of Antwerp in Belgium on the other hand. The Lake Baikal area is dominated by the influence of the massive fresh water reserves and can be characterized by low population density, limited industrial activities and boreal forests. The Antwerp area on the other hand is located in one of the most densely populated regions in Europe, Flanders, where a concentration of road transport, industrial as well as agricultural activities give rise to high aerosol concentrations, notably in the form of elevated concentrations of PM_{10} and $PM_{2.5}$ (Deutsch *et al*., 2008a). Being at the cross road of European North-South and East-West transportation routes, transport emissions are dominant contributors of $PM_{2.5}$ and PM_{10} in the Antwerp ambient atmosphere. Traffic emissions are also found to be the main source of Ultra Fine Particles (UFP) in urban areas (Avino *et al.*, 2011). Especially the semi-volatile PM fraction of these emissions is highly correlated with the toxicological potency of PM (Ning and Sioutas, 2010). Antwerp also includes one of the largest harbor areas in the world where a large number of refineries are present, resulting in elevated SO_2 emissions, which are of particular interest in this study.

The focus of this paper is on the (numerical) formulation of the model as well as on its implementation. The applications are shown in the first place to demonstrate this implementation and show its generic aspects. However, in the case of Lake Baikal, measurements were available to compare with model results and thus validate the model in

* Corresponding author. Tel.: ++32.14.33.67.00;
Fax: ++32.14.32.11.85
E-mail address: clemens.mensink@vito.be

some respect. In the Antwerp case, no specific aerosol measurements were available, but the concentration patterns obtained in this study could be compared with model validation studies focusing on the formation and transport of PM_{10}, $PM_{2.5}$ and other air substances (Deutsch *et al.*, 2008b).

The paper is structured in the following way. Section 2 describes in detail the set up of the model, i.e. the governing model equations are presented needed to simulate the aerosol formation, aerosol transport, and gas-aerosol interactions. Numerical aspects of implementing the model are also included in this section. Section 3 presents the results of the model application for Lake Baikal and for the Antwerp area. Results are discussed by evaluating and comparing the number concentrations obtained for the different situations.

METHODOLOGY AND MODEL SETUP

For the simulation of aerosol formation processes, chemistry induced substances are very critical. Their vapor super-saturation leads to the formation of primary clusters serving as a basis for aerosol formation. Then, these substances may interact with the nuclei from the background atmosphere and merge with water drops of definite sizes, with the subsequent coagulation of these particles.

A key role in atmospheric disperse systems is played by sulfate aerosols. These atmospheric particles can have both direct and indirect impact on the climate system. They can be found in different parts of the atmosphere: free troposphere, marine boundary layer, and arctic areas. Numerical and field studies indicate that new sulfate particles can be nucleated in the stratosphere and polluted urban air (Clarke, 1992; Wexler *et al.*, 1994; Schroder and Strom, 1997; Kulmala *et al.*, 1998; Aloyan *et al.*, 2002). Most studies predict that new-particle formation is due to binary homogeneous nucleation (for example, between water and sulfuric acid) (Seinfeld and Pandis, 1998; Kulmala *et al.*, 2000).

The behavior of gas-phase admixtures is characterized by the formation of hydrates of water and sulfuric acid, when one acid molecule and one or more water molecules combine to form fine clusters (Kulmala *et al.*, 1998; Vehkamäki *et al.*, 2002). However, a detailed description of nucleation thermodynamics and kinetics in three-dimensional models requires huge computational resources. In view of this, we employed a parameterized nucleation model with an adequate prediction of the nucleation rate (Noppel, 1998; Vehkamäki *et al.*, 2002).

At present, there are many models for aerosol dynamics as described among others by Aloyan *et al.* (1993), Wexler *et al.* (1994), Aloyan *et al.* (1997), Piskunov *et al.* (1997), Ackermann *et al.* (1998), Meng *et al.* (1998), Aloyan (2000), Piskunov (2000). Most three-dimensional models for aerosol dynamics assume an instantaneous equilibrium in the gas-aerosol system. However, as shown by Aloyan *et al.* (1993), Meng *et al.* (1998) and Piskunov (2000), under some conditions, the equilibrium is reached quite slowly when compared to the time scale of other processes. Therefore, it is necessary to develop numerical models using a non-uniform distribution function. Another key requirement to the models is that conservation laws for particle mass and number are satisfied.

In most cases, the particle size distribution is parameterized. For example, in Ackermann *et al.* (1998), the distribution of aerosols generated through primary emission and gas-phase oxidation of sulfur dioxide is represented by a pair of lognormal modes. The parameters of these distributions are obtained from transport equations written for the zeroth, third, and sixth moments of each mode. The main mechanism of nucleation is taken to be the homogeneous nucleation of drops of sulfuric acid and water. Some models of aerosol dynamics use a generalized approach allowing the aerosol spectrum to be described by a simple analytical function (lognormal, gamma-distribution, mono-disperse spectrum, etc.). In this case, one or two parameters (or moments) of the spectrum are calculated. Compared to the generalized approach, the direct approach is more accurate in describing the evolution of the particle size spectrum, but requires considerable computational resources, because the spectrum needs to be split into many intervals (Aloyan *et al.*, 1993; Wexler *et al.*, 1994; Aloyan *et al.*, 1997; Piskunov *et al.*, 1997; Meng *et al.*, 1998; Aloyan and Piskunov, 2005). In each case, the choice of an approach depends on the purpose of the study and the availability of accompanying resources.

Because the regional-scale processes of aerosol dynamics proceed in the turbulent atmosphere and, for the most part, the Earth's surface is orographically and thermally inhomogeneous, the dynamics of gaseous admixtures and aerosols should be modeled using the thermo-hydrodynamic equations for meso-scale atmospheric processes.

Thus, the regional model for atmospheric gas-aerosol dynamics incorporates the following modules: thermo-hydrodynamics, transport and photochemical transformation of gaseous admixtures, dynamics of sulfuric-acid aerosols generated through primary emission and gas-phase oxidation of sulfur dioxide, binary homogeneous nucleation, and kinetic processes of condensation/evaporation and coagulation. The basic models for the description of the spatio-temporal variations in concentrations of gaseous admixtures and aerosols can be found in Aloyan *et al.* (1993), Aloyan *et al.* (1997), Piskunov *et al.* (1997), Aloyan (2000) and Aloyan and Piskunov (2005).

Basic Model Equations

The model is based on the thermo-hydrodynamic equations for meso-scale atmospheric processes in the non-hydrostatic approximation, taking into account the processes of moisture exchange and atmospheric interaction with the underlying surface that has thermal and orographic inhomogeneities. The orography is treated through a terrain-following transformation from the Cartesian system of coordinates (x, y, z) to a generalized system $(\overline{x}, \overline{y}, \sigma)$ by the formulas $\overline{x} = x$, $\overline{y} = y$, $\sigma = (z - \tilde{\delta}(x, y)) / H - \tilde{\delta}(x, y))\hat{H}$, where $\tilde{\delta}(x, y)$ is a function describing the relief of the Earth's surface and H and $\hat{H}$ are the upper boundaries of the model domain in the Cartesian and generalized system of coordinates, respectively.

The thermodynamic variables are represented as the

sums of two terms: $\vartheta = \Theta(z) + \vartheta'(x, y, z, t)$, $q = Q(z) + q'(x, y, z, t)$, $p = P(z) + p'(x, y, z, t)$, $\rho = P(z) + \rho'(x, y, z, t)$, where ϑ is the potential temperature, q is the specific humidity, p is pressure, and ρ is the air density. Here, the capital letters denote the large-scale components of meteorological variables and their deviations are denoted by primes.

In the new system of coordinates, the hydrodynamic equations in the Boussinesq approximation take the following form (Aloyan, 1992; Aloyan *et al.*, 1995; Aloyan, 2008):

$$\frac{\partial \hat{u}}{\partial t} + divu\hat{u} = -\frac{\partial p'}{\partial x} + a_1 \frac{\partial p'}{\partial \sigma} + l(\hat{v} - \hat{V}_{bckg}) + F_u + a_3^2 \frac{\partial}{\partial \sigma} \rho \nu_u \frac{\partial}{\partial \sigma}\left(\frac{\hat{u}}{\rho}\right) \quad (1)$$

$$\frac{\partial \hat{v}}{\partial t} + divu\hat{v} = -\frac{\partial p'}{\partial y} + a_2 \frac{\partial p'}{\partial \sigma} - l(\hat{u} - \hat{U}_{bckg}) + F_v + a_3^2 \frac{\partial}{\partial \sigma} \rho \nu_u \frac{\partial}{\partial \sigma}\left(\frac{\hat{v}}{\rho}\right) \quad (2)$$

$$\frac{\partial \hat{w}}{\partial t} + divu\hat{w} = -a_3 \frac{\partial p'}{\partial \sigma} + \lambda \hat{\vartheta}'(1 + \gamma q) + F_w + a_3^2 \frac{\partial}{\partial \sigma} \rho \nu_u \frac{\partial}{\partial \sigma}\left(\frac{\hat{w}}{\rho}\right) \quad (3)$$

$$\frac{\partial \hat{\vartheta}'}{\partial t} + divu\hat{\vartheta}' + \frac{S}{a_3}(\hat{w} + \tilde{\delta}_x \hat{u} + \tilde{\delta}_y \hat{v}) = \frac{L_w \Phi \overline{\rho}}{C_p} + F_\vartheta + a_3^2 \frac{\partial}{\partial \sigma} \rho \nu_\vartheta \frac{\partial}{\partial \sigma}\left(\frac{\hat{\vartheta}'}{\rho}\right) + Q_r \quad (4)$$

$$\frac{\partial \hat{q}'}{\partial t} + divu\hat{q}' = -a_3 \hat{w} \frac{\partial Q}{\partial \sigma} - \Phi \overline{\rho} + F_q + a_3^2 \frac{\partial}{\partial \sigma} \rho \nu_q \frac{\partial}{\partial \sigma}\left(\frac{\hat{q}'}{\rho}\right) \quad (5)$$

$$\frac{\partial \hat{u}}{\partial x} + \frac{\partial \hat{v}}{\partial y} + \frac{\partial \hat{w}}{\partial \sigma} = 0 \quad (6)$$

The following notation is used:

$$a_1 = \tilde{\delta}_x \frac{\sigma - H}{H - \tilde{\delta}(x, y)}, \quad a_2 = \tilde{\delta}_y \frac{\sigma - H}{H - \tilde{\delta}(x, y)}, \quad a_3 = \frac{H}{H - \tilde{\delta}(x, y)},$$
$$divu\hat{\varphi} = \frac{\partial u\hat{\varphi}}{\partial x} + \frac{\partial v\hat{\varphi}}{\partial y} + \frac{\partial w\hat{\varphi}}{\partial \sigma}, \quad \hat{\varphi} = \rho\varphi, \quad \varphi = (u, v, w, \vartheta, q)$$
$$\tilde{\delta}_x = \frac{\partial \tilde{\delta}}{\partial x}, \quad \tilde{\delta}_y = \frac{\partial \tilde{\delta}}{\partial y}, \quad \omega = a_1 u + a_2 v + a_3 w, \quad (7)$$
$$F_u = \frac{\partial \tau_{11}}{\partial x} + \frac{\partial \tau_{12}}{\partial y} + \frac{\partial}{\partial \sigma}(a_1 \tau_{11} + a_2 \tau_{12}),$$
$$F_v = \frac{\partial \tau_{21}}{\partial x} + \frac{\partial \tau_{22}}{\partial y} + \frac{\partial}{\partial \sigma}(a_1 \tau_{21} + a_2 \tau_{22}),$$
$$F_w = \frac{\partial \tau_{31}}{\partial x} + \frac{\partial \tau_{32}}{\partial y} + \frac{\partial}{\partial \sigma}(a_1 \tau_{31} + a_2 \tau_{32}),$$
$$F_\vartheta = \frac{\partial H_1}{\partial x} + \frac{\partial H_2}{\partial y} + \frac{\partial}{\partial \sigma}(a_1 H_1 + a_2 H_2),$$

where t is time; u, v, and w are the wind-velocity components along x, y, σ axes, respectively; $u = (u, v, w)$; $\hat{\delta}(x, y)$ is the function describing the Earth's topography; l is the Coriolis parameter; L_w is the latent heat of condensation; Φ is the rate of moisture condensation; S is the stratification parameter; $\lambda = g/T$ is the buoyancy parameter; Q_r is the radiative heat influx; $\gamma = 0.61$; $\overline{\rho}(z)$ is the background density; τ_{ij} is the Reynolds stress tensor; H_i and Q_i are the turbulent fluxes of heat and moisture, respectively ($i = \overline{1,3}; j = \overline{1,3}$); and ν_u, ν_ϑ, ν_q are the vertical turbulent exchange coefficients for the moments of momentum, heat, and moisture, respectively.

The structure of the surface air layer is described by the Monin-Oboukhov similarity theory and the Businger empirical functions (Businger *et al.*, 1971). For strong instability conditions, the vertical profiles of meteorological fields in the surface layer are approximated by the 1/3 law and, for strong stability, a linear relationship is used.

The system of Eqs. (1)–(6) is solved in the domain

$$D_t = D \times [0, T], \; D = \left\{ \begin{matrix} (x, y, \sigma) : x \in [-X, X], \\ y \in [-Y, Y], \sigma \in [0, H] \end{matrix} \right\}$$

under the following initial and boundary conditions

$$\hat{u} = \hat{v} = \hat{w} = 0, \; \hat{\vartheta}' = 0, \; \hat{q}' = 0 \;\text{ for } t = 0 \quad (8)$$

$$\frac{\partial \hat{u}}{\partial x} = \frac{\partial \hat{v}}{\partial x} = \frac{\partial \hat{w}}{\partial x} = 0, \; \frac{\partial \hat{\vartheta}}{\partial x} = 0, \; \frac{\partial \hat{q}}{\partial x} = 0 \;\text{ for } \; x = \pm X \quad (9)$$

$$\frac{\partial \hat{u}}{\partial y} = \frac{\partial \hat{v}}{\partial y} = \frac{\partial \hat{w}}{\partial y} = 0, \; \frac{\partial \hat{\vartheta}}{\partial y} = 0, \; \frac{\partial \hat{q}}{\partial y} = 0 \;\text{ for } \; y = \pm y \quad (10)$$

$$\hat{u} = \hat{U}_{bckg}, \hat{v} = \hat{V}_{bckg}, \hat{w} = 0, \; \hat{\vartheta}' = 0, \; \hat{q}' = 0 \;\text{ for } \; \sigma = H \quad (11)$$

$$a_3 h \frac{\partial \hat{u}}{\partial \sigma} = a_u \hat{u}, \; a_3 h \frac{\partial \hat{v}}{\partial \sigma} = a_u \hat{v}, a_3 h \frac{\partial \hat{\vartheta}}{\partial \sigma} = a_\vartheta (\hat{\vartheta} - \hat{\vartheta}_0),$$
$$a_3 h \frac{\partial \hat{q}}{\partial \sigma} = a_\vartheta (\hat{q} - \hat{q}_0), \frac{\hat{w}}{h} = -\left(\frac{\partial \hat{u}}{\partial x} + \frac{\partial \hat{v}}{\partial y}\right) \quad (12)$$
$$\text{for } \; \sigma = \frac{h - \tilde{\delta}(x, y)}{H - \tilde{\delta}(x, y)} H$$

$$\hat{\omega}' = 0 \quad \text{for } \sigma = 0, \quad (13)$$

where a_u and a_θ are functions determined from the surface-

layer model and h is the height of the underlying surface, U_{bckg} and V_{bckg} are the background values of velocity at the upper boundary of the boundary layer (geostrophic wind). The temperature over the water surface is assumed to be given, and the specific humidity is computed by the Magnus formula (Matveev, 1967). The Earth's surface temperature is calculated from the combined solution of the heat balance equation and the equation of heat conduction in soil.

Parametrization of Subgrid-Scale Turbulent Diffusion

Averaging over the volume of a reference grid cell in the thermo-hydrodynamic equations yields common terms describing the sub-grid scale Reynolds stress. Following Gal-Chen and Sommerville (1975), the symmetric stress tensor τ_{ij} is represented as a function depending on the deformation $D_{i,j}$ of average motion:

$$\tau_{ij} = \bar{\rho} \nu_M D_{ij}, \tag{14}$$

where

$$D_{ij} = \frac{\partial u_i}{\partial x_j} + \frac{\partial u_j}{\partial x_i} - \frac{2}{3}\frac{\delta_{ij}}{\delta_{ii}} \nabla u_i, \ \left(i = \overline{1,3};\ j = \overline{1,3}\right), \tag{15}$$

where δ_{ij} is the Kronecker delta: $\delta_{ij} = 1$ if $i = j$ and $\delta_{ij} = 0$ if $i \neq j$. The heat flux is determined by the formula

$$H = \bar{\rho} \nu_\vartheta \delta_{ii} \frac{\partial \vartheta}{\partial x_j}. \tag{16}$$

here, ν_M and ν_θ are the coefficients of kinematic viscosity and diffusion, respectively. Eqs. (14)–(16) use tensor notations. The spatiotemporal variations of the parameter ν_M are determined from the following closure scheme

$$\nu_M = \begin{cases} \left(\tilde{K}\bar{\Delta}\right)^2 |Def|, & Ri > 1 \\ \left(\tilde{K}\bar{\Delta}\right)^2 |Def| \left(1 - \frac{\nu_\vartheta}{\nu_u} Ri\right), & Ri \le 1 \end{cases} \tag{17}$$

where $\bar{\Delta} = A^{1/3}$, $A = \Delta x\, \Delta y\, \Delta z$ is the volume of a reference grid cell, and $\tilde{K} = 0.21$. The deformation (Def) is defined as

$$\left(Def\right)^2 = \frac{1}{2}\left(D_{11}^2 + D_{22}^2 + D_{33}^2 + D_{12}^2 + D_{13}^2 + D_{23}^2\right). \tag{18}$$

The Richardson number (Ri) is represented as

$$Ri = \frac{\frac{g}{\Theta}\frac{\partial \vartheta}{\partial z}}{\left(Def\right)^2} \tag{19}$$

Modeling the Transport of Pollutants in the Atmosphere

The equations of transport of multicomponent gaseous admixtures and aerosols can be represented as (Aloyan, 2000; Aloyan and Piskunov, 2005; Aloyan, 2008)

$$\frac{\partial C_i}{\partial t} + u_j \frac{\partial C_i}{\partial x_j} = F_i^{gas} - J - P_i^{cond} + P_i^{phot} + \frac{\partial}{\partial x_j} K_{jj} \frac{\partial C_i}{\partial x_j}, \quad (j = \overline{1,3}) \tag{20}$$

$$\frac{\partial \phi_k}{\partial t} + (u_j - \delta_{j3} w_g) \frac{\partial \phi_k}{\partial x_j} = F_k^{aer} + J + P_k^{cond} + P_k^{coag} + \frac{\partial}{\partial x_j} K_{jj} \frac{\partial \phi_i}{\partial x_j}, \quad (j = \overline{1,3}) \tag{21}$$

where $(x_1 = x, x_2 = y, x_3 = z)$, $(u_1 = u, u_2 = v, u_3 = w)$; C_i, $i = 1, \ldots, N_g$, and φ_k, $k = 1, \ldots, N_a$, are the concentrations of gaseous admixtures and aerosols, respectively; N_g and N_a are the numbers of the corresponding components; w_g is the gravitational settling; F_{gas} and F_{aer} are the emissions of gaseous admixtures and aerosols, respectively; J, P_{cond}, P_{coag}, and P_{phot} are the operators of nucleation, condensation, coagulation, and photochemical transformation, respectively.

Eqs. (20) and (21) are solved in the domain

$$D_t = D \times [0,T],\ D = \left\{ \begin{matrix} (x,y,z) : x \in [-X,X], \\ y \in [-Y,Y],\ z \in [0,H] \end{matrix} \right\}$$

under the following initial and boundary conditions

$$C_i = C_i^0, \quad \phi_i = \phi_i^0, \quad \text{at } t = 0,$$

$$C_i = C_i^b, \quad \phi_i = \phi_i^b, \quad \text{at } z = H.$$

At the lateral boundaries of the domain, the following boundary conditions are used:

$$C_i\big|_\Gamma = C_i^b,\ \phi_i\big|_\Gamma = \phi_i^b, \text{ if } u_n < 0,$$

$$\left.\frac{\partial C_i}{\partial n}\right|_\Gamma = 0,\ \left.\frac{\partial \phi_i}{\partial n}\right|_\Gamma = 0, \text{ if } u_n \ge 0,$$

where Γ is the lateral surface, n is the outer normal to Γ, and u_n is the normal component of the wind velocity. The values of the functions C_i^b and ϕ_i^b are given values (background fields).

To set the boundary condition at $z = h$, the surface resistance of an admixture is represented as the sum of three terms: aerodynamic resistance (r_a); quasi-laminar surface-layer resistance (r_b), conditioned by molecular diffusion processes near the Earth's surface; and surface resistance (r_c), conditioned by processes on the deposition surface. Thus, the admixture flux in the surface layer is given in the form

$$\nu \frac{\partial C_i}{\partial z} = \frac{C_i - C_{i,surf}}{r_a + r_b + r_c}, \tag{22a}$$

where $r_b = \frac{2}{\kappa u_*}\left(\frac{Sc}{Pr}\right)^{2/3}$ for gaseous species,

$$\nu\frac{\partial\phi_k}{\partial z} = \frac{\phi_k - \phi_{k,surf}}{r_a + r_b + r_a r_b w_g} + \mathrm{w_g}\phi_\mathrm{k}, \quad (22b)$$

for aerosol particles [29].

here, $\boldsymbol{\kappa} = 0.4$ is the von Kármán constant, $Sc = 1.5 \times 10^{-5}$ is the Schmidt number, $Pr = 0.71$ is the Prandtl number, and u_* is the friction velocity.

Modeling Photochemical Processes

We suppose that the following gaseous admixtures are emitted into the atmosphere: {NO, NO_2, CO, CH_4, H_2CO, SO_2}. Chemical reactions initiated by sunlight lead to the formation of new chemically active atoms, free radicals, and other species, which, together with the primary emissions, constitute the following system: {$O(^1D)$, $O(^3P)$, O_3, OH, HO_2, H, H_2O, NO_3, NO, NO_2, SO_2, H_2CO, HCO, H_2O_2, CO, CH_4, HNO_2, HNO_3, SO_3, H_2SO_4, SO_2^*, N_2O_5, CH_3, CH_3O_2, CH_3O, CH_3OH, CO_2, $CH_3O_2NO_2$, HCOOH, $HOCH_2O$, $HOCH_2O_2$, CH_3OOH, HO_2NO_2, CH_3ONO_2, isoprene, etc.}. The photochemical model incorporates a total of 204 chemical reactions among 36 gas constituents, typical of the atmospheric nitrogen, sulfur, and carbon cycles (Aloyan *et al.*, 1995; Aloyan *et al.*, 2003; Aloyan *et al.*, 2004; Aloyan, 2005). It should be noted that the formation of nucleation-mode particles involves only water vapor and sulfuric acid particles.

Modeling the H_2O–H_2SO_4 Homogeneous Nucleation

Suppose that, in the supersaturated vapor at temperature T and at pressure P_v, the atmosphere contains a binary cluster consisting of n_w molecules of the substance w and n_a molecules of the substance a with the mole fractions x_{iv}, $i = (w, a)$. We assume that the particles have a spherical shape and are in a liquid phase. Then, the free energy for the formation of a new liquid particle in the binary mixture can be represented as (Wilemski, 1984)

$$W = \Delta G = n_w\Delta\mu_w + n_a\Delta\mu_a + A\sigma, \quad (23)$$

where ΔG is the variation of the Gibbs free energy, A is the surface area, σ is the surface tension, $\Delta\mu_i = \mu_{il}(T, P_v, x_{il}) - \mu_{iv}(T, P_v, x_{iv})$, where μ_{il} and μ_{iv} are the chemical potentials in the liquid and vapor phases, respectively. It should be noted that, for a supersaturated vapor, the function ΔG has a maximum at the point of critical radius r^*. Vapor is supersaturated for all drops with $r > r^*$ (Noppel, 1998; Vehkamäki *et al.*, 2002).

The radius of the critical cluster (r^*) and the free energy for critical-cluster formation (w^*) are determined as

$$r^* = \frac{2\sigma(x^*)v_i(x^*)}{kT\ln\left(\rho_i^{free}\Big/\rho_{i,s}^{free}(x^*)\right)}; \quad (24)$$

$$w^* = \frac{4}{3}\pi r^{*2}\sigma(x^*). \quad (25)$$

Finally, the expression for the nucleation rate takes the form

$$J = Z\rho(1,2)\exp\left[-\frac{w^* - w(1,2)}{kT}\right], \quad (26)$$

where $\rho(1,2)$ and $w(1,2)$ are the number concentration and the formation energy of sulfuric acid di-hydrate, respectively, and Z is a kinetic coefficient. Here, the di-hydrate is used as an initial size (i.e., as a reference point for distributions).

Kinetic Modeling of Condensation and Coagulation Processes

First, let us consider coagulation processes. Some problems of atmospheric physics require the consideration of particles consisting of a mixture of different substances (composite particles). In modeling the coagulation kinetics of these particles, one has to solve system (27) which is based on the Smoluchowski equation. If the term α in (27) is disregarded, the classical Smoluchowski equation is obtained (Smoluchowski, 1916). Composite particles are formed in the atmosphere (for example, in acid precipitation and deposition of gaseous admixtures onto aerosol particles). In this case, one has to consider the kinetic equations for two-component systems. In the case of spatial uniformity, the kinetic equation of coagulation can be written as (Piskunov *et al.*, 1997; Piskunov, 2000; Aloyan and Piskunov, 2005)

$$\frac{\partial C(g,\alpha,t)}{\partial t} = \frac{1}{2}\int_0^g\int_0^\alpha K(g-s,\alpha-\beta;s,\beta)C(g-s,\alpha-\beta)C(s,\beta)ds\,d\beta - C(g,\alpha,t)\int_0^\infty\int_0^\infty K(g,\alpha;s,\beta)C(s,\beta)ds\,d\beta, \quad (27)$$

where g is the total mass of particles, α is the mass of emitted admixtures, K is the coagulation coefficient, and $C(g, \alpha, t)$ is the total concentration of particles.

The additional variable α appearing in Eq. (27) significantly hinders the solution of the problem. If the coagulation nuclei are taken to be independent of the presence of admixtures in specific particles (i.e., $K = K(g, s)$), this leads to a considerable simplification of problem solution (Piskunov *et al.*, 1997). It should be noted that the coagulation kernels depend not only on the geometric size of particles, but also on the densities of colliding particles, which is especially true at the initial stage of the process, when the interaction between admixture particles and a passive fraction is very active. To take this effect into account, one can consider the mean contribution of admixture to the density, given by the term $\overline{\alpha(g,t)}$ (Piskunov *et al.*, 1997):

$$K(g, \alpha; s, \beta) \cong K[g, \overline{\alpha(g,t)}\,; s, \overline{\beta(s,t)}\,] \equiv k(g, s, t). \quad (28)$$

Problem (28) is solved using the following integral parameters as basic characteristics of the particle spectrum:

$$n(g,t) = \int_0^g C(g,\alpha,t)d\alpha\,;\ m(g,t) = \int_0^g \alpha C(g,\alpha,t)d\alpha\,. \quad (29)$$

Now, let us separate explicitly the contributions of admixtures and composite particles to the total concentration:

$$C(g, \alpha, t) = c(g, t)\,\delta(g - \alpha) + c_c(g, \alpha, t) \quad (30)$$

where $c(g, \alpha, t)$ is the concentration of admixture particles with a total mass g and an admixture mass α, $c_c(g, \alpha, t)$ is the concentration of composite particles, α is the mass of substance (admixture) in the particle. Inserting Eq. (30) into (27) and using integral parameters (29), we obtain the system of coupled equations (Piskunov *et al.*, 1997)

$$\frac{\partial n(g,t)}{\partial t} = \frac{1}{2}\int_0^g K(g-s,s)n(g-s)n(s)ds - n(g)\int_0^\infty K(g,s)n(s)ds \quad (31)$$

$$\frac{\partial m(g,t)}{\partial t} = \frac{1}{2}\int_0^g K(g-s,s)n(g-s)m(s)ds - m(g)\int_0^\infty K(g,s)n(s)ds \quad (32)$$

$$\frac{\partial c(g,t)}{\partial t} = \frac{1}{2}\int_0^g K(g-s,s)n(g-s)m(s)ds - c(g)\int_0^\infty K(g,s)n(s)ds \quad (33)$$

Numerical Aspects of Solving the Coagulation Equation

In line with Eq. (30), we represent the particle number $n(g)$ and mass $m(g)$ concentrations in the form

$$n(g) = n_c(g) + c(g)\,;\ m(g) = m_c(g) + gc(g)\,. \quad (34)$$

To solve Eqs. (31)–(33), the grids

$$\omega_c = \{\tilde{g}_1 = 0, \tilde{g}_2, \cdots, \tilde{g}_L\}\,,\ \omega = \{g_1 = 0, g_2, \cdots, g_j\} \quad (35)$$

are specified for the composite fraction and admixture, respectively.

By ν_j, we denote the number of admixture particles in the interval (g_j, g_{j+1}); by N_{ci}, the number of composite particles in the interval $(\tilde{g}_i, \tilde{g}_{i+1})$; and, by I_{ci}, the mass of admixture particles in composite particles in the interval $(\tilde{g}_i, \tilde{g}_{i+1})$:

$$\nu_i = \int_{g_j}^{g_{j+1}} c dg\,;\ N_{ci} = \int_{\tilde{g}_i}^{\tilde{g}_{i+1}} n_c dg\,;\ I_{ci} = \int_{\tilde{g}_i}^{\tilde{g}_{i+1}} m_c dg\,. \quad (36)$$

These are the basic mesh functions. To derive equations for these, we assume that $c(g)$, $n_c(g)$, and $m_c(g)$ are piecewise-constant functions in the mesh intervals ω and ω_c:

$$c(g) = \frac{\nu_j}{g_{j+1} - g_j}\,,\ n_c(g) = \frac{N_{ci}}{g_{i+1} - g_i}\,,\ m_c(g) = \frac{I_{ci}}{g_{i+1} - g_i}\,,\ g_j < g < g_{j+1}\,. \quad (37)$$

The coagulation kernels are also assumed to be piecewise-constant functions of two variables. Under these assumptions for the form of the functions $c(g)$ and $n_c(g)$, the particle mass concentrations for the integral grids ω and ω_c have the following form:

$$\mu_{j+1} = \int_{g_j}^{g_{j+1}} \mathrm{gcd}\, g = \nu_j \frac{g_j + g_{j+1}}{2}\,, \quad (38)$$

$$N_{c,i+1} = \int_{\tilde{g}_i}^{\tilde{g}_{i+1}} g n_c dg = N_{ci} \frac{\tilde{g}_j + \tilde{g}_{j+1}}{2}\,. \quad (39)$$

Now, let us multiply Eqs. (31)–(33) by g and integrate over the interval (g_{i-1}, g_{i+1}). The system of equations for ν_j, N_{ci}, I_{ci} can be represented as (Piskunov *et al.*, 1997)

$$\frac{d\nu_j}{dt} = \frac{1}{2}F(\nu_1, \cdots, \nu_j) - \nu_j \sum_{p=1}^{J-1} k_{jp}\nu_p - \nu_j \sum_{p=1}^{L-1} k_{jp} N_{cp}\,,\ 1 \le j \le J-1 \quad (40)$$

$$\frac{dN_{ci}}{dt} = \frac{1}{2}F(N_{c1}, \cdots, N_{ci}) - N_{ci}\sum_{p=1}^{J-1} k_{ip}\nu_p - N_{ci}\sum_{p=1}^{L-1} k_{ip} N_{cp} + \tilde{F}(N_{c1}, \cdots, N_{ci}, \nu_1, \cdots, \nu_{pi}), \quad (41)$$

$$\frac{dI_{ci}}{dt} = \bar{F}(N_{c1}, \cdots, N_{ci}, I_{c1}, \cdots, I_{ci}, \nu_1, \cdots, \nu_{pi}) - I_{ci}\sum_{p=1}^{J-1} k_{ip}\nu_p - I_{ci}\sum_{p=1}^{L-1} k_{ip} N_{cp} \qquad 1 \le i \le L-1 \quad (42)$$

here, $F, \bar{F}, \tilde{F}$ are some quadratic functions with their coefficients depending on coagulation kernels. After its discretization, the system of Eqs. (40)–(42) is solved by an iterative method. When the local computation of the coagulation process is completed, c and n can be used as initial values for the condensation process. Based on the mean content of admixture in each particle, one can calculate the mass of the core (the core is assumed to be the substance with its mass in the composite particle equal to $g - \alpha$):

$$g_{p0} = g - \bar{\alpha}\,;\ \overline{\alpha(g,t)} = m_c(g,t) \Big/ n_c(g,t) \quad (43)$$

In describing the condensation kinetics, the mass of the core in particles can be taken to be constant. Therefore, we assume that the condensation values of c_c, n_c, and m_c are related in the following way (here, g_{po} is the mass of core in the particle at the initial time step of condensation):

$$c_c(g,\alpha,t) = n_c(g,t)\delta(g - g_{po} - \alpha);$$
$$m_c(g,t) = (g - g_{po})n_c(g,t). \quad (44)$$

The kinetic equations of condensation for the distribution functions c and n are

$$\frac{\partial c}{\partial t} + \frac{\partial}{\partial g}\left(v_g c\right) = J(g,t)\delta\left[g - g_*(t)\right];$$
$$\frac{\partial n_c}{\partial t} + \frac{\partial}{\partial g}\left(v_g n_c\right) = 0 \quad (45)$$

where v_g is the growth rate of particles with a total mass of g, J is the nucleation rate, and g_* is the mass of the critical-size drop. The numerical algorithm for solving problem (45) can be found in Aloyan *et al.* (1993) and Piskunov *et al.* (1997). In Eq. (45), the binary nucleation rate is given according to the algorithm described above. An example of its practical application can be found in Aloyan (2000), Aloyan (2008) and, partially, in Aloyan and Arutyunyan (2004).

RESULTS AND DISCUSSION

Results for the Lake Baikal Area

Using the models described above, numerical experiments were performed to investigate the spatio-temporal variations of gaseous admixtures and aerosols in the Lake Baikal region. The calculations were performed for the following input parameters: a 600 × 600 km modeling domain with a horizontal resolution of 10 km; the upper boundary of the domain is fixed at a height of 2050 m from the Earth's surface; the number of vertical levels is 20 (Δz = 50 m if $z \le 100$ m; Δz = 75 m if $100 \le z \le 250$ m; Δz = 100 m if $250 \le z \le 1450$ m; and Δz = 150 m if $1450 \le z \le 2050$ m); and the time step is 600 s. The start of simulations corresponded to 6 h local time. The characteristics of the background flow were U_b = 4 m/s and V_b = 0 at the upper boundary of the atmosphere (z = 2050 m). These conditions reflect the characteristics of a single given day and should not necessarily coincide with the dominating background flow in the region. The figures shown below outline the Lake Baikal region with its large industrial point emission sources indicated by circles: (1) Shelekhov (Heat Power Plant-5), (2) Irkutsk (Novoirkutsk Heat Power Plant, RK Novolenino), (3) Angarsk (Heat Power Plant-1, Heat Power Plant-9, Heat Power Plant-10), (4) Baikal'sk, and (5) Usol'e (Heat Power Plant-11). The SO_2 emission magnitudes (g/s) for these five points (together with their corresponding heights) are as follows: (1) Shelekhovo: 156 g/s (z = 130 m); (2) Irkutsk: 311 g/s (z =50 m), 400 g/s (z = 90 m), 378 g/s (z =130 m); (3) Angarsk: 5400 g/s (z = 90 m), 860 g/s (z = 130 m), 430 g/s (z = 190 m); (4) Baikalsk: 281 g/s (z = 90 m); (5) Usole: 195 g/s (z = 50 m), 501 g/s (z = 90 m). The structure of NO_x and CO emissions is similar to SO_2. Dominant emission sources are point 3 (Angarsk) for NO_x and point 2 (Irkutsk) for CO. With the use of the data of SO_2, NO_x, and CO emissions from these sources, numerical experiments were performed to reproduce the spatio-temporal variations of gaseous admixtures and aerosols in the atmosphere. The calculations were performed simultaneously within the combined model in the following way. Using the hydrodynamic model, the atmospheric circulation characteristics, wind flow field, and turbulence parameters for the Lake Baikal region were calculated. Fig. 1 shows the wind flow field in the (x, y) plane at a height of 250 m for t = 14 h local time (LT). Against the background of the atmospheric circulation patterns obtained, the problem of admixture transport and photochemical transformation was solved leading to the formation of sulfuric acid (H_2SO_4) and other secondary pollutants. Then, new-particle formation was simulated through the binary nucleation mechanism in the H_2O–H_2SO_4 system. And, finally, aerosol particle dynamics was simulated with allowance for the kinetic processes of condensation/evaporation and coagulation. In this case, both natural aerosol spectra (for example, the Junge distribution) and nucleation-induced particles are involved in condensation/evaporation. The experiment includes a total of 30 particle-size bins in the range from 0.003 to 4 μm. Along with nucleation-mode particles generated from precursor gases, the model deals also with background aerosol (particles with a diameter of 0.1 to 4.0 μm, given by a Junge distribution). The main aim of our paper is to study the gas-aerosol interaction and formation of nucleation-mode particles (in the H_2SO_4–H_2O system). The study of the gaseous composition of the atmosphere without consideration of aerosols has been performed earlier (Aloyan *et al.*, 1995, 2003). It is clear that the photochemical processes significantly affect the concentrations of such species as $O(^1D)$,$O(^3P)$, OH, HO_2, which in turn affect the concentrations of stable species (and particularly, H_2SO_4). In Fig. 2, the H_2SO_4 concentration field is shown for t = 22 h LT. Fig. 3 shows the H_2SO_4 threshold concentration field. Note that the new-particle formation is possible only if the concentration of sulfuric acid vapors exceeds the threshold value. As one can see from Fig. 2, for the given time, the threshold value in the Baikal region was exceeded, which assists in the formation of fine aerosol particles. We also calculated the sensitivity of the nucleation rate J (cm^3/s), critical radius r_* (nm), and H_2SO_4 threshold concentration to temperature and specific-humidity variations. For example, at T = 265 K and $[H_2SO_4] = 10^9$ cm^{-3}, we have $J = 2.8 \times 10^5$ cm^3/s and $r_* = 0.55$ nm for a relative humidity of RH = 50% and $J = 1.8 \times 10^6$ cm^3/s and $r_* = 0.52$ nm for a relative humidity of RH = 90%, while, at T = 281 K, we have J = 0.4 cm^3/s and $r_* = 0.66$ nm for a relative humidity of RH = 50% and $J = 1.4 \times 10^3$ cm^3/s and $r_* = 0.6$ nm for a relative humidity of RH = 90%. Thus, decreasing temperature leads to increased nucleation rates and decreased radii of the critical cluster, while decreasing specific humidity reverses the situation. Clearly, the H_2SO_4 threshold concentration increases with temperature and decreases with increasing

specific humidity. Fig. 4 demonstrates the number concentrations of aerosol particles with radii 0.025 μm (Fig. 4(a)), 0.1 μm (Fig. 4(b)), and 0.915 μm (Fig. 4(c)) for t = 22 h LT and at z = 250 m. The calculation results indicate that the field of aerosol particle concentrations may undergo dramatic spatio-temporal variations.

Fig. 5 shows a comparison between the calculated and measured values of the concentration of nucleation-mode particles in Listvyanka (NIFHI measurement data for the Baikal area) (Dal Maso *et al.*, 2007). Fig. 5 refers to nucleation in the sulfuric acid-water system only. We can note that particles below 30 nm in size can be generated only as a result of chemical and photochemical reactions from precursor gases, because the rise of dust particles from the surface is hampered by van-der-Waals forces. The oxidation of SO_2 as a precursor was shown to play a key role in new particle formation (see Fig. 5). The discrepancies between experimental and calculated data are explained by the existence of alternative channels for the formation of nucleation-mode particles. There has been no clear understanding of alternative nucleation mechanisms (apart from H_2SO_4–H_2O). The consistency between experimental and calculated data may become better by taking into account ammonia, free ions, and, possibly, low-volatile organic compounds. However, these nucleation mechanisms have been poorly studied and were not included into the given model. Yet, the comparison results given in Fig. 5 show that the H_2SO_4–H_2O binary homogeneous

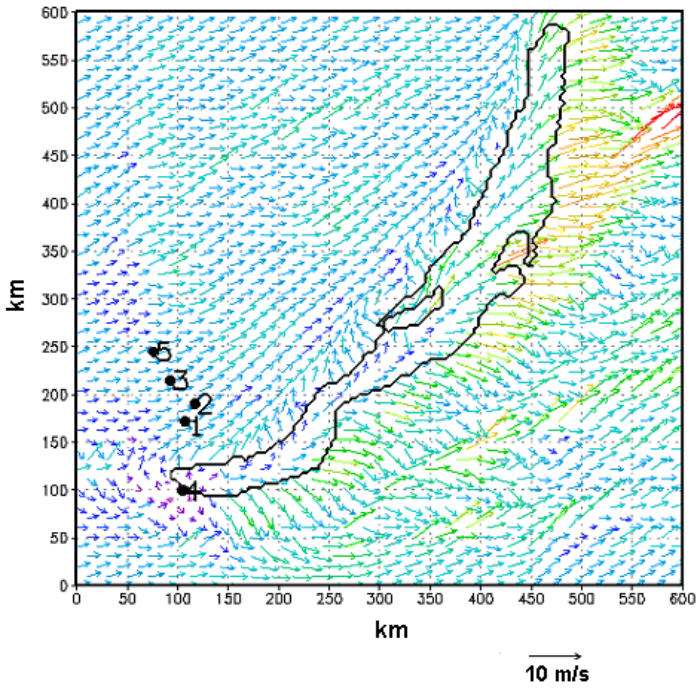

Fig. 1. Wind velocity field (m/s) in the (x, y) plane of Lake Baikal, Russia, at a height of 250 m and for t = 14 h LT.

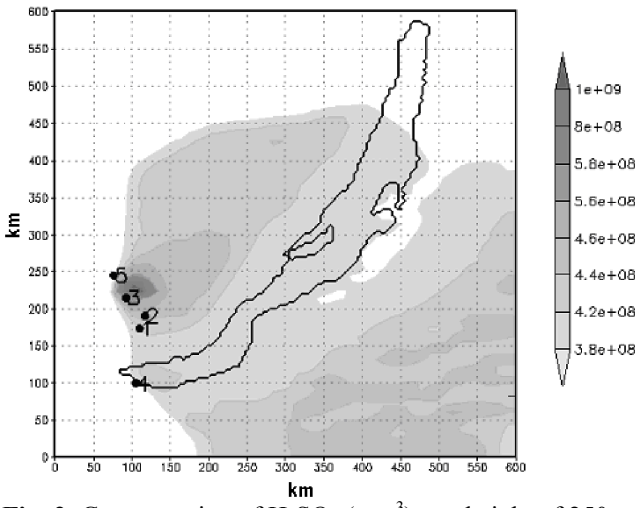

Fig. 2. Concentration of H_2SO_4 (cm^{-3}) at a height of 250 m and for t = 22 h LT at Lake Baikal, Russia.

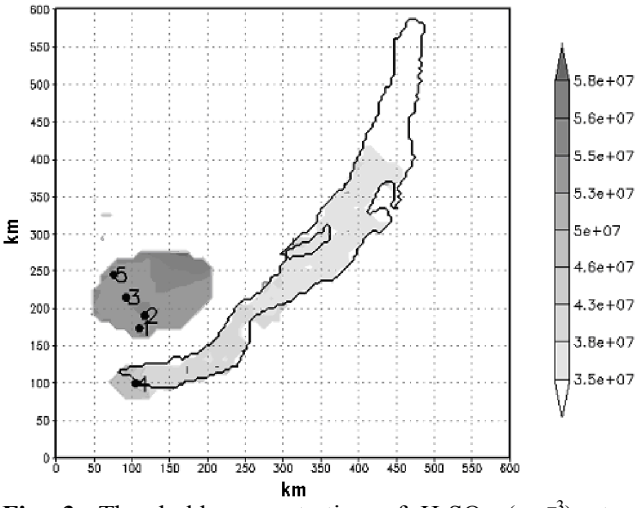

Fig. 3. Threshold concentration of H_2SO_4 (cm^{-3}) at a height of 250 m and for t =22 h LT at Lake Baikal, Russia.

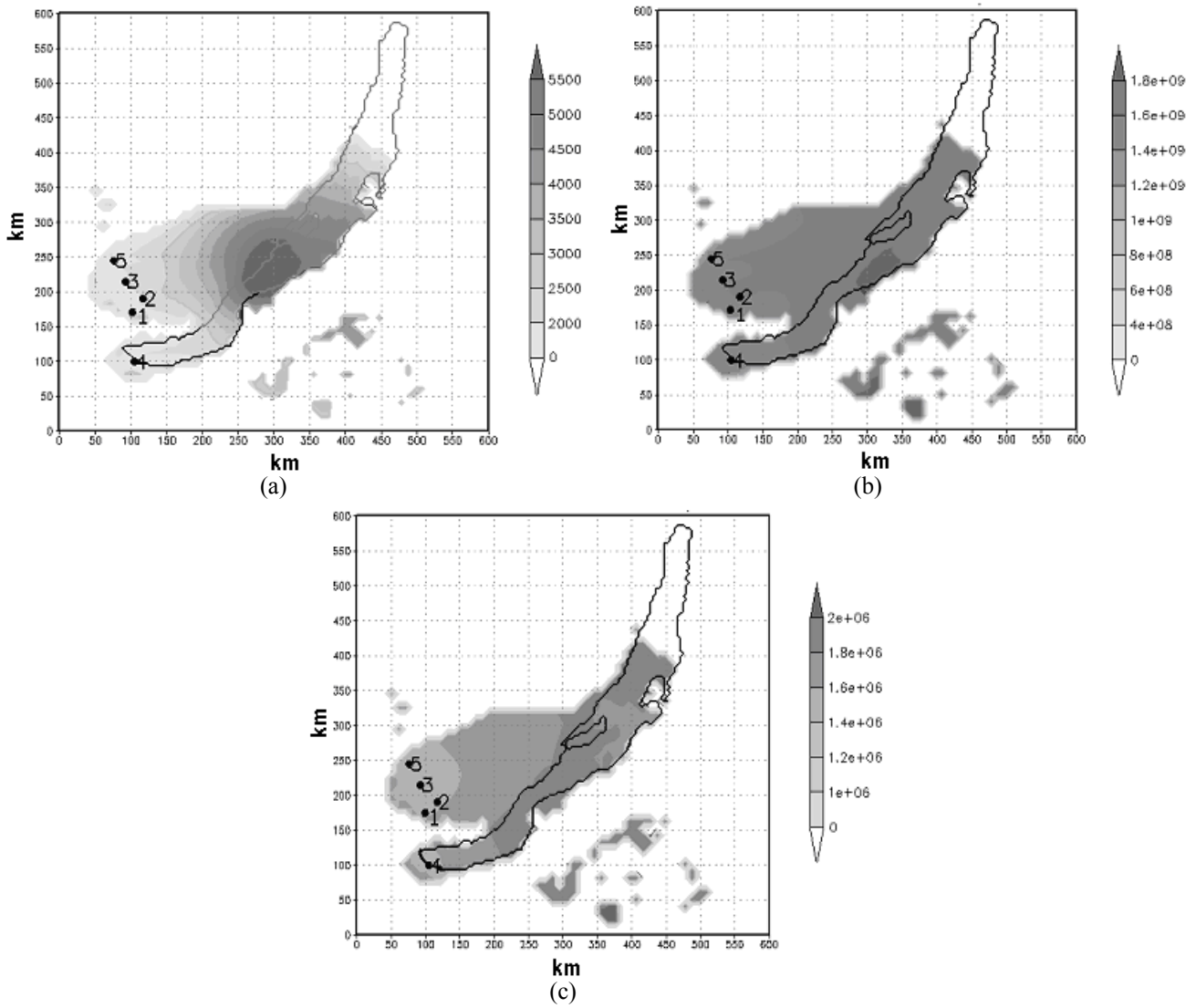

Fig. 4. Number concentrations of aerosol particles (m^{-3}) with radii (a) 0.025, (b) 0.1, and (c) 0.915 μm at a height of 250 m and for a 24-h model run for Lake Baikal, Russia.

nucleation plays a rather significant, although not exclusive, role in the formation of nucleation-mode particles. Our choice of binary nucleation of water vapor and sulfuric acid is conditioned by extremely low pressures of sulfuric acids over water solutions due to almost complete ionization (dissociation) of its molecules as well as by the fact that no ammonia emission data were available for the Baikal region thus excluding the use of a ternary nucleation mechanism in our model calculations. Then, the newly formed sulfate particles are assumed to interact with background aerosol (having regard to their size distributions), which leads to variations in the number concentration of submicron-sized aerosol particles. The above-mentioned discrepancies serve to improve the model nucleation mechanism through the involvement of additional individual components. For example, according to measurement data, from 20 to 50% of nucleation-mode particles are charged particles, which may arise from natural radioactivity and/or radon emissions in the given region.

Results for the Antwerp Area

The second class of numerical experiments is related to the modeling of gas and aerosol variability in the Antwerp area in Belgium. Meteorological data (wind field, temperature, specific humidity, turbulence characteristics) prepared at VITO were used in the chemical model to calculate the secondary air pollution of the area conditioned by photochemical transformations, advection, and turbulent diffusion (Deutsch *et al.*, 2008c). The aerosol formation model is applied with a prior calculation of nucleation rates, threshold concentration of sulfuric acid and radii of critical clusters at each point of the 3D domain. The binary/ternary homogeneous nucleation model uses given data of SO_2, H_2O, and NH_3 concentrations, as well as temperature and relative humidity. Then, the kinetic model of condensation/evaporation and coagulation is used to calculate the variation of aerosol particle-size distribution in the range between 2 nm and 4 μm.

The numerical experiments were performed under the

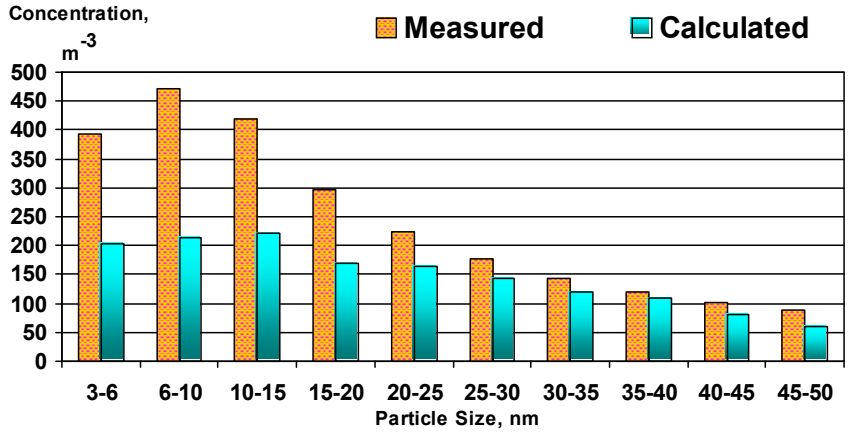

(a) Listvyanka, 26.08.2003, t = 12 h

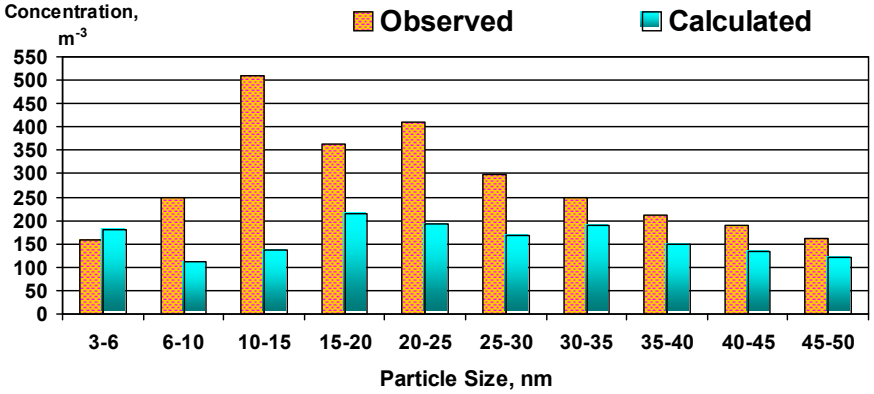

(b) Listvyanka, 26.08.2003, t = 15 h

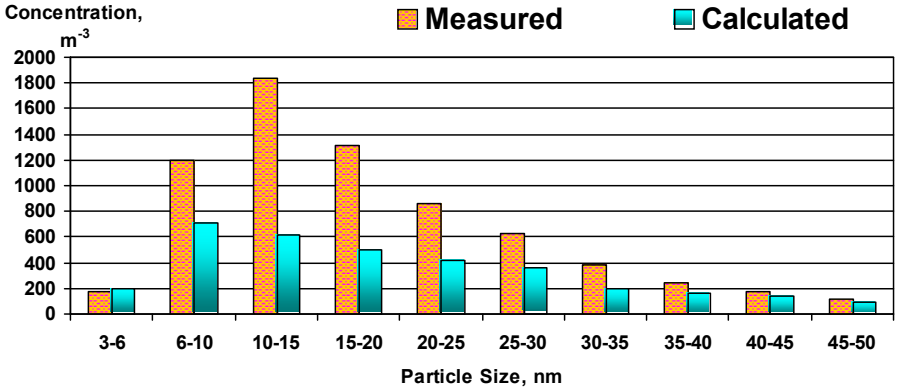

(c) Listvyanka, 26.08.2003, t = 24 h

Fig. 5. Comparison between calculated and measured data (NIFHI) for Lake Baikal, Russia.

following input parameters: dimensions of the modeling domain were 40 km × 40 km in the horizontal (with a step size of 1 km) and 3.5 km in the vertical (15 levels of variable heights), the time step was 10 min. The domain includes the City of Antwerp and its harbor area. The geographical coordinates of the central point of the modeling domain are 51.23°N latitude and 4.43°E longitude. The emission data of the gaseous species SO_2, NO, NO_2, CO, H_2CO, isoprene, etc. (mole/m^2 s) used in the calculations were obtained as in Deutsch *et al.* (2008c). The model takes into account 12 types of the underlying surface. The time interval of numerical calculations is three days of December 2003, and the start time corresponds to t_0 = 6 h local time (LT).

The results of the numerical experiments indicate that in some areas of the modeling domain enhanced values of SO_2 and NH_3 concentrations and relative humidity lead to a strong new-particle formation from precursor gases. Fig. 6 shows the aerosol concentration fields in the (*x, y*) plane at different heights (28 m (a), 309 m (b), and 910 m (c)) for t = t_0 + 6h LT. It can be seen from here that there is an intense formation of nucleation-mode particles of radius of 2 nm in different parts of the domain, with their concentrations reaching up to 10^6 cm^{-3}. Fig. 7 is the same except for particles with radius of 8 nm. Figs. 8 and 9 are the same as Figs. 6 and 7, respectively, except for midnight at t = t_0 + 18h LT. Here, due to decreased photochemistry, the number

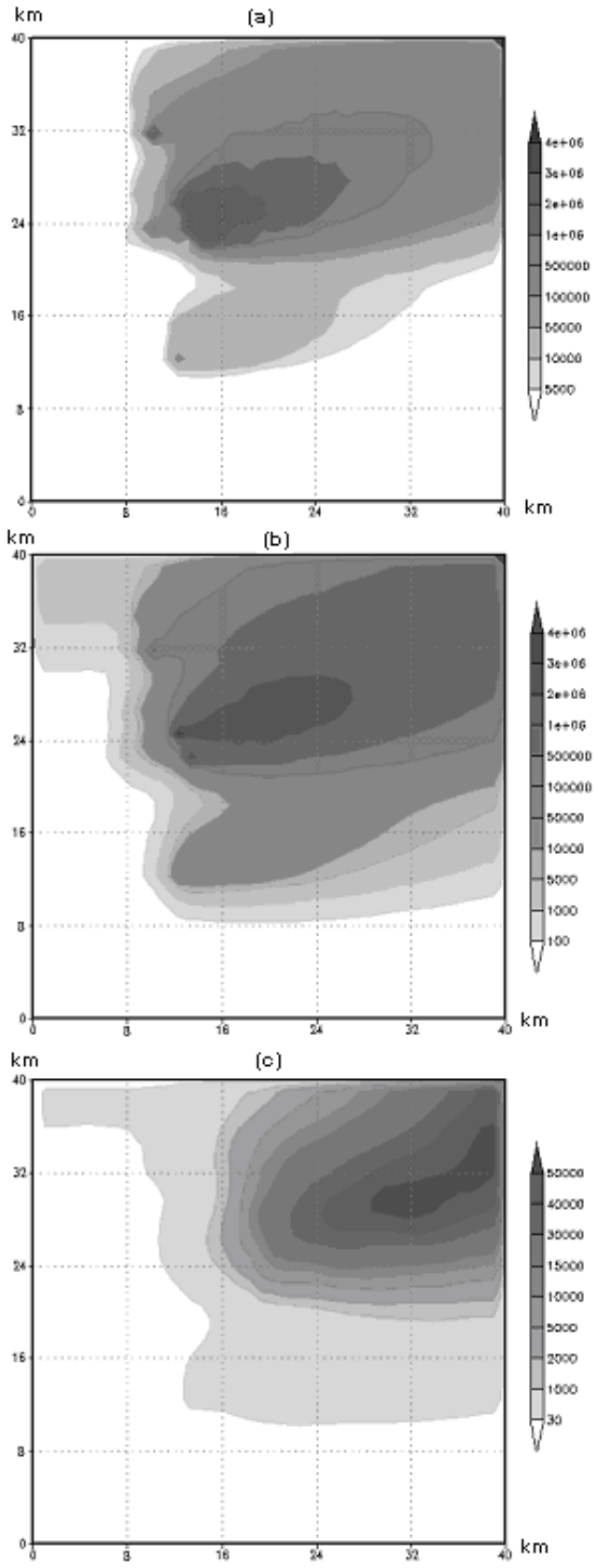

Fig. 6. Aerosol (particles of 2 nm of radius) concentration (m^{-3}) in the (*x, y*) plane at $t = t_0 + 6$ h LT at different heights: 28 m (a), 309 m (b), and 910 m (c) for the Antwerp area, Belgium

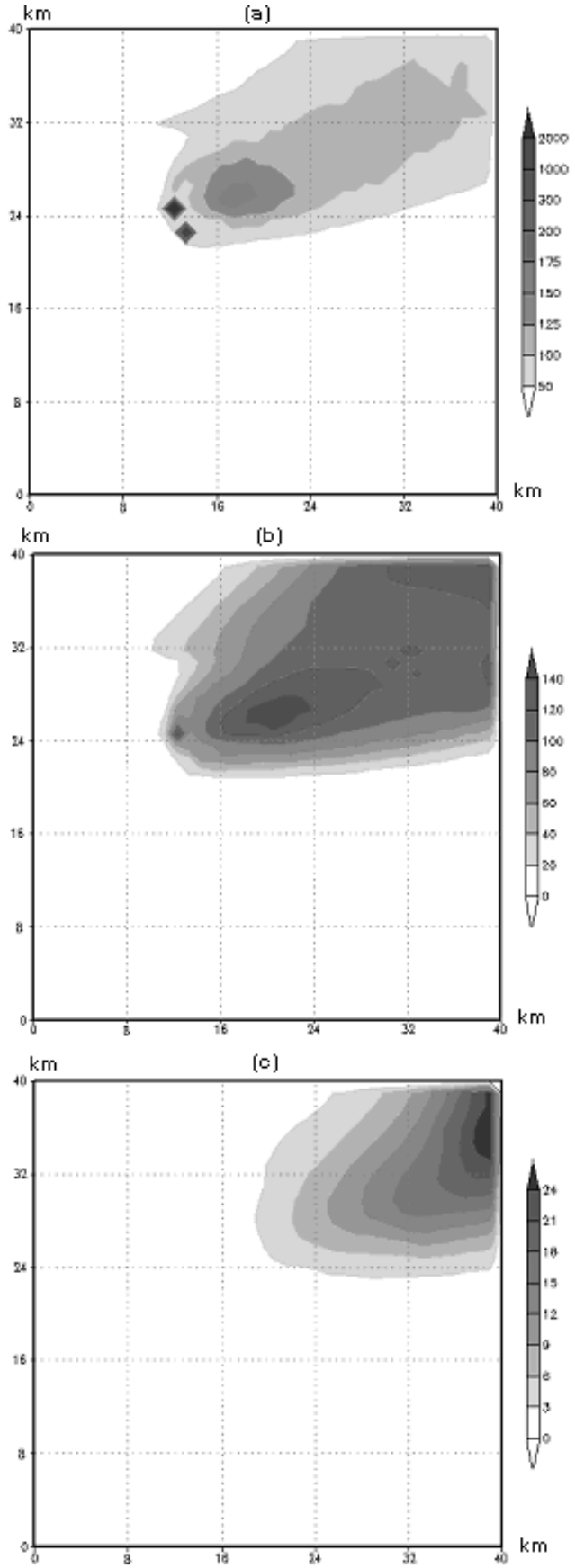

Fig. 7. Same as Fig. 6 except for aerosol particles of 8 nm of radius.

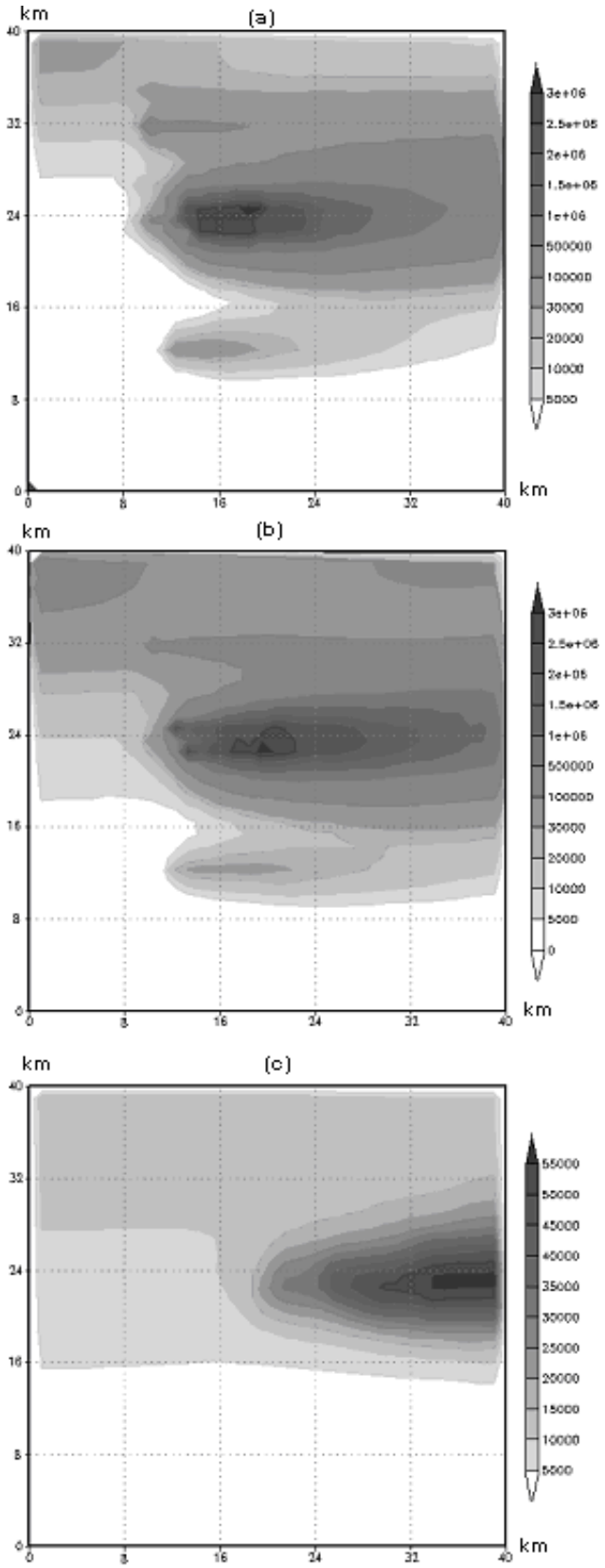

Fig. 8. Aerosol (particles of 2 nm of radius) concentration (m^{-3}) in the (*x, y*) plane $t = t_0 + 18$ h LT at different heights: 28 m (a), 309 m (b), and 910 m (c) for the Antwerp area, Belgium (the central point of the modeling domain: 51.23°N by latitude and 4.43°E by longitude).

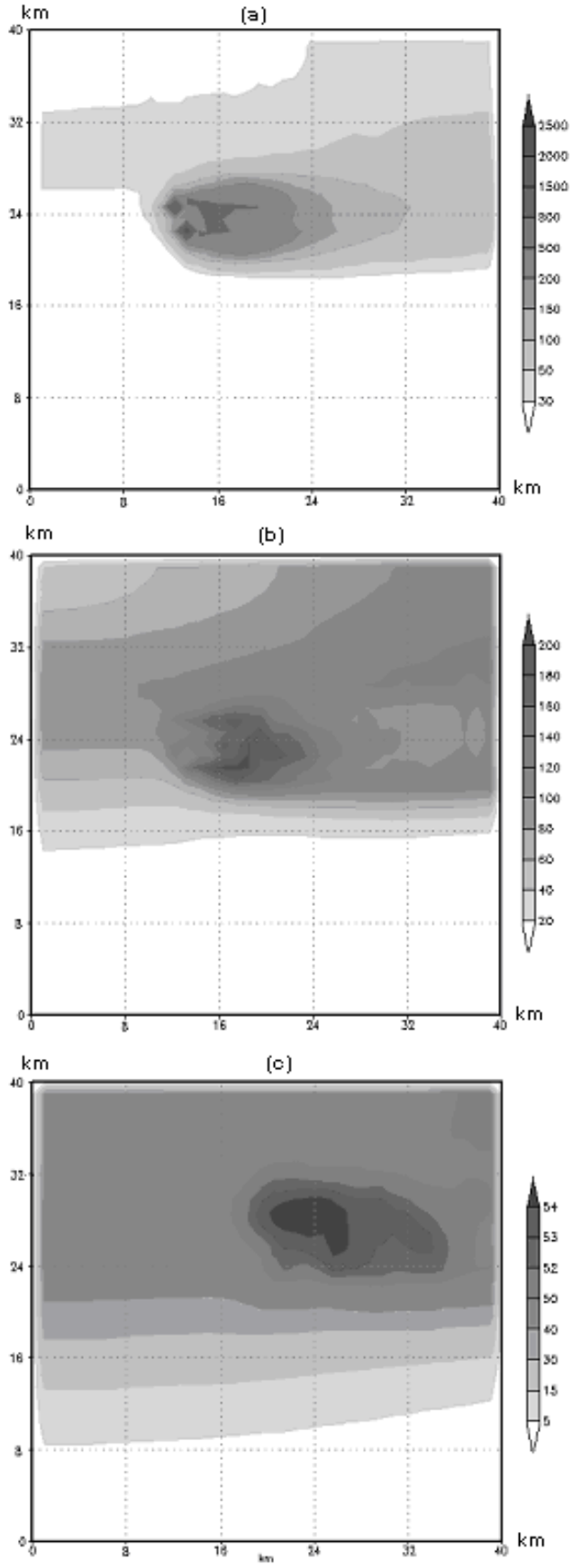

Fig. 9. Same as Fig. 8 except for aerosol particles of 8 nm of radius.

concentrations of the corresponding particles are significantly smaller. At nighttime, the sulfuric acid concentration is practically vanishing and no nucleation occurs: only condensational growth and inter-mode coagulation between particles can be traced. With time, due to coagulation and condensation, the particle-size distribution is expanded to form larger (sub-micron size and more) particles. Fig. 10 presents the aerosol concentrations for the whole size spectrum at $t = t_0 + 24$ h LT at a single point with grid coordinates (16, 24, 3). Due to increased H_2SO_4 concentrations and relative humidity, the new-particle formation is strong. Fig. 11 shows the concentrations of H_2SO_4 at a height of 360 m for time instants: at $t = t_0 + 12$ h LT (Fig. 11(a)) and at $t = t_0 + 24$ h LT (Fig. 11(b)). In these cases, the H_2SO_4 concentrations are essentially higher than the threshold concentration necessary for the generation of small-size particle clusters. Fig. 11 shows the H_2SO_4 concentrations (molecules/cm^3) calculated for daytime and morning periods. These data illustrate again the significance of photochemical transformations in the formation of H_2SO_4 in the atmosphere. For a more detailed study of the photochemical effect (taking into account the diurnal course) on aerosols, additional numerical experiments are required, which can be analyzed in a new paper aimed specifically at studying the sensitivity of concentrations of nucleation-mode particles to variations in the chemical reaction rates conditioned by the diurnal course. Note that similar data as applied to specific regions can be found in (Aloyan *et al.*, 1995, 2003). As can be seen from the above figures the Antwerp atmosphere is characterized by an intense formation of nucleation-mode particles, which may significantly affect the spatial and temporal variability of SO_2 and H_2SO_4 concentrations as well as the aerosol particle-size distribution.

CONCLUSIONS

For the given regions, detailed reliable measurement data to be compared with calculation results are missing. This is especially the case for aerosol particle emissions from point and area sources.

Despite the fact that more and more measurement techniques become available to cover a wide spectrum in the size distributions of aerosols (e.g., as reported by Liu *et al.*, 2010), measurements for the lower end of the spectrum are still very difficult to obtain. This is especially the case for more routinely based measurements of particle emission of diesel vehicles (Rostedt *et al.*, 2009), that would be needed to verify the model results for the Antwerp application. Therefore, the results of the numerical experiments presented in this paper are merely of exploratory character. However, specific modules of the model described above were verified using measurement data. In particular, a comparison between calculated and observed data is performed for the results of the photochemical model (Aloyan *et al.*, 2004) and the aerosol model (Aloyan *et al.*, 1997). The models considered can be used to solve a wide range of environmental problems related to the investigation of the regional-scale spatio-temporal dynamics of gaseous admixtures and aerosols in the atmosphere. The numerical experiments show that nucleation-mode particles can be formed in the boundary layer in the example of the Lake Baikal region. It was also shown that new-particle formation in the atmosphere is largely based on the mechanism of binary homogeneous nucleation in the water-sulfuric acid system. The results of numerical experiments indicate that the Antwerp area is characterized by an intense formation of nucleation-mode particles due to increased values of SO_2 and H_2SO_4 concentrations and relative humidity.

ACKNOWLEDGEMENTS

This study was supported by the RFBR, under projects 06-05-65184 and 06-05-66861.

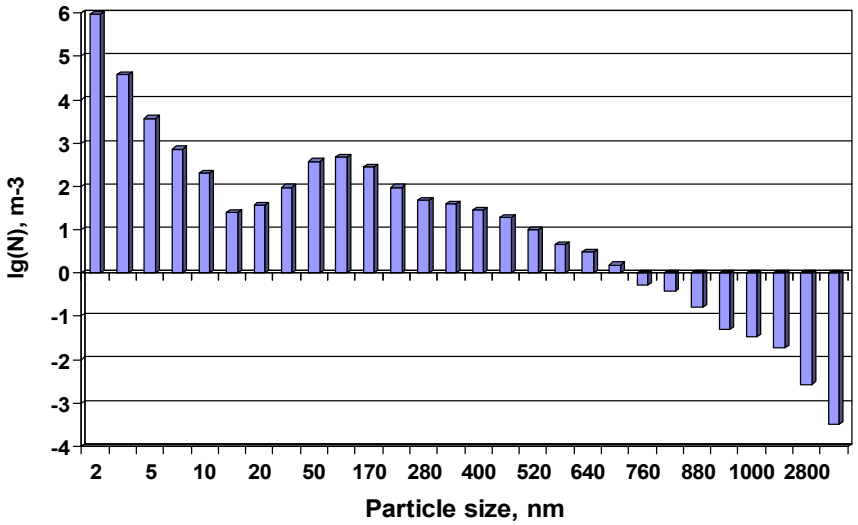

Fig. 10. Aerosol concentrations (m^{-3}) (logarithmic scale) for the particle size spectrum between 2 nm and 3.4 μm at $t = t_0 + 24$ h LT at the grid point with coordinates (16, 24, 3) for the Antwerp area, Belgium (the central point of the modeling domain: 51.23°N by latitude и 4.43°E by longitude).

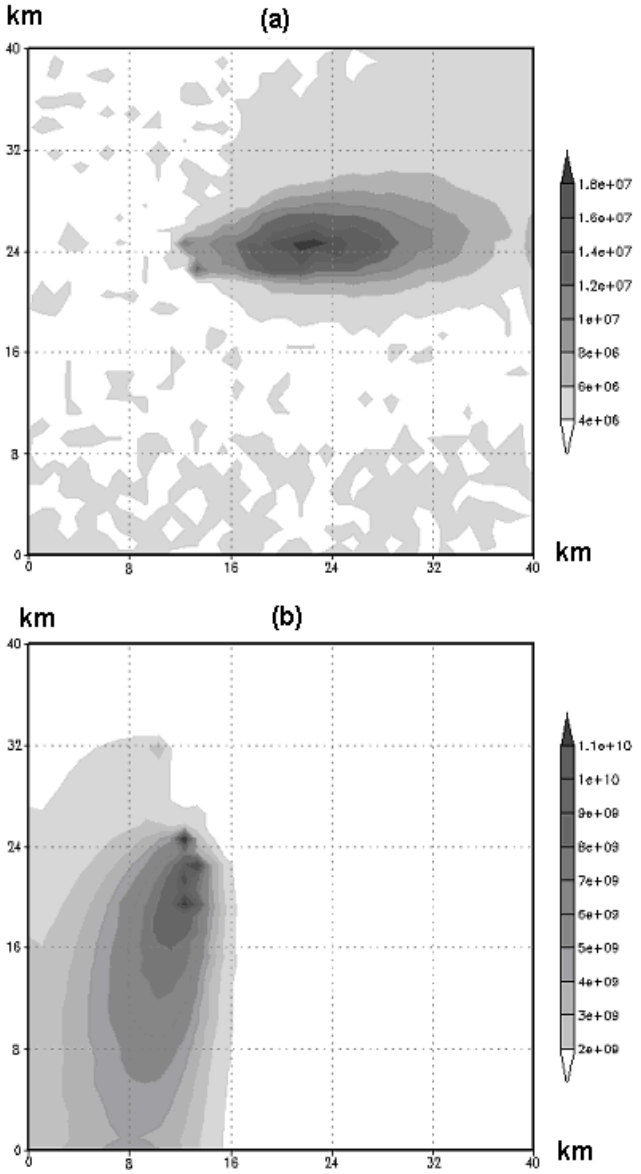

Fig. 11. Concentrations of H_2SO_4 (cm^{-3}) at z = 360 m after $t = t_0 + 12$ h LT (a) at $t = t_0 + 24$ h LT (b) of calculations for the Antwerp area, Belgium (the central point of the modeling domain: 51.23°N by latitude и 4.43°E by longitude).

REFERENCES

Ackermann, I.J., Hass, H., Memmesheimer, M., Ebel, A., Binkowski, F.S. and Shankar, U. (1998). MADE: Modal Aerosol Dynamics Model for Europe: Development and First Applications. *Atmos. Environ.* 32: 2981–2999.

Aloyan, A.E. (1992). A Non-Hydrostatic Numerical Model of Mesoscale Atmospheric Layer Response. *Russ. J. Num. Anal. Math. Model.* 7, 371–386.

Aloyan, A.E., Egorov, V.D., Marchuk, G.I. and Piskunov, V.N. (1993). Aerosol Formation Mathematical Modelling with Consideration for Condensation Kinetics. *Russ. J. Num. Anal. Math. Model.* 7: 457–472.

Aloyan, A.E., Arutyunyan, V.O. and Marchuk, G.I. (1995). Dynamics of Mesoscale Boundary Atmospheric Layer and Impurity Spreading with the Photochemical Transformation Allowed for. *Russ. J. Num. Anal. Math. Model.* 10: 93–114.

Aloyan, A.E., Arutyunyan, V.O., Lushnikov, A.A. and Zagaynov, V.A. (1997). Transport of Coagulating Aerosol in the Atmosphere. *J. Aerosol Sci.* 28: 67–85.

Aloyan, A.E. (2000). Numerical Modeling of the Interaction of Gas Species and Aerosols in the Atmospheric Dispersive Systems. *Russ. J. Num. Anal. Math. Model.* 15: 211–224.

Aloyan, A.E., Arutyunyan, V.O. and Louzan, P.I. (2002). Numerical Modeling of the Gas-Aerosol Interaction in the Atmosphere, Proc. ENVIROMIS-2002, Gordov, E. and Tomsk, V.I., (Eds.), IOM SB RAS, p. 158–164.

Aloyan, A.E., Arutyunyan, V.O., Haymet, A.D., He, J.W., Kuznetsov, Y. and Lubertino, G. (2003). Air Quality Modeling for Houston-Galveston-Brazoria Area. *Environ. Int.* 29:377–383.

Aloyan, A.E. and Arutyunyan, V.O. (2004). Mathematical Modeling of the Regional-Scale Variability of Gaseous Species and Aerosols in the Atmosphere, In *Advances in Air Pollution Modelling for Environmental Security,* Farago, I., Georgiev, K. and Havasi, A. (Eds.), Borovetz.

Aloyan, A.E., Arutyunyan, V.O., Kuznetsov, Y.A. and He, J.W. (2004). Modeling the Regional Transport and Photochemical Transformation of Gaseous Admixtures in the Atmosphere. *Izv. RAN. FAO* 40: 441–453.

Aloyan, A.E. and Piskunov, V.N. (2005). Modeling the Regional Dynamics of Gaseous Admixtures and Aerosols. *Izv. RAN. FAO* 41: 1–13.

Aloyan, A.E. (2008). *Modeling the Dynamics and Kinetics of Gas Pollutants and Aerosols in the Atmosphere,* Nauka, Moscow.

Avino, P., Casciardi, S., Fanizza, C. and Manigrasso, M. (2011). Deep Investigation of Ultrafine Particles in Urban Air. *Aerosol Air Qual. Res.* 11: 654–663.

Businger, J.A., Wyngard, I.C., Izumi, Y. and Bradley, E.F. (1971). Flux-Profile Relationships in the Atmospheric Surface Layer. *J. Atmos. Sci.* 28: 181–189.

Clarke, A.D. (1992). Atmospheric Nuclei in the Remote Free Atmosphere. *J. Atmos. Chem.* 14: 479–488.

Dal Maso, M., Sogacheva, L., Vlasov, A., Staroverova, A., Lushnikov, A., Anisimov, M., Zagaynov, V.A., Khodzher, T.V., Obolkin, V.A., Lyubotseva, Yu. S., Riipinen, I., Kerminen, V.M. and Kulmala, M. (2007). Aerosol Particle Formation Events at Two Siberian Stations, In *Nucleation and Atmospheric Aerosols*, O'Dowd C.D. and Wagner, P.E. (Eds.), Springer, p. 840–844.

Deutsch, F., Vankerkom, J., Janssen, L., Janssen, S., Bencs, L., Van Grieken, R., Fierens, F., Dumont, G. and Mensink, C. (2008a). Modelling Concentrations of Airborne Primary and Secondary PM_{10} and $PM_{2.5}$ with the BelEUROS Model in Belgium. *Ecol. Modell.* 217: 230–239.

Deutsch, F., Janssen, L., Vankerkom, J., Lefebre, F. and Mensink, C. (2008b). Modelling Changes of Aerosol Composition over Belgium and Europe. *Int. J. Environ. Pollut.* 32: 162–173.

Deutsch, F., Mensink, C., Vankerkom, J. and Janssen, L.

(2008c). Application and Validation of a Comprehensive Model for PM_{10} and $PM_{2.5}$ Concentrations in Belgium and Europe. *Appl. Math. Model.* 32: 1501–1510.

Gal-Chen, T. and Somerville, C.J. (1975). Numerical Solution of the Navier-Stokes Equations with Topography. *J. Comput. Phys.* 17: 276–310.

Kulmala, M., Laaksonen, A. and Pirjola, L. (1998). The Potential for Atmospheric Mixing Processes to Enhance the Binary Nucleation Rate. *J. Geophys. Res*. 103: 8301–8307.

Kulmala, M., Pirjola, L. and Mäkelä, J.M. (2000). Stable Sulphate Clusters as a Source of New Atmospheric Particles. *Nature* 404: 66–69.

Liu, B.Y.H., Romay, F.J., Dick, W.D., Woo, K.S. and Chiruta, M. (2010). A Wide-Range Particle Spectrometer for Aerosol Measurement from 0.010 μm to 10 μm. *Aerosol Air Qual. Res.* 10: 125–139.

Matveev, L.T. (1967). *Fundamentals of General Meteorology: Physics of the Atmosphere*, IPST, Jerusalem.

Meng, Z., Dabdub, D. and Seinfeld, J.H. (1998). Size-Resolved and Chemically Resolved Model of Atmospheric Aerosol Dynamics. *J. Geophys. Res*. 103: 3419–3435.

Ning, Z. and Sioutas, C. (2010). Atmospheric Processes Influencing Aerosols Generated by Combustion and the Inference of Their Impact on Public Exposure: A Review. *Aerosol Air Qual. Res.* 10: 43–58.

Noppel, M. (1998). Binary Nucleation of Water-Sulfuric Acid System: A Re-examination of the Classical Hydrates Interaction Model. *J. Chem. Phys*. 109: 9052–9056.

Piskunov, V.N., Golubev, A.I., Goncharov, E.A. and Ismailova, N.A. (1997). Kinetic Modeling of Composite Particles Coagulation. *J. Aerosol Sci*. 28: 1215–1231.

Piskunov, V.N. (2000). *Theoretical Models of Aerosol Formation Kinetics*, VNIIIEF, Sarov.

Rostedt, A., Marjamäki, M., Ojanperä, J-Y., Keskinen, J., Janka, K., Niemelä, V. and Ukkonen, A. (2009) Non-Collecting Electrical Sensor for Particle Concentration Measurement. *Aerosol Air Qual. Res.* 9: 470–477.

Schroder, F. and Strom, J. (1997). Aircraft Measurements of Sub-Micrometer Aerosol Particles (< 7 nm) in the Midlatitude Free Troposphere and Tropopause Region. *Atmos. Res*. 44: 333–356.

Seinfeld, J.H. and Pandis, S.N. (1998). *Atmospheric Chemistry and Physics: From Air Pollution to Climate Change*, Wiley, New York.

Smoluchowski, M.V. (1916). Drei Vorträge über Diffusion, Brownsche Bewegung und Koagulation von Kolloidteilchen. *Physik. Zeit*. 17: 557–585.

Vehkamäki, H., Kulmala, M., Napari, I., Lehtinen, K.E.J., Timmreck, C., Noppel, M. and Laaksonen, A. (2002). An Improved Parameterization for Sulfuric Acid/Water Nucleation Rates for Tropospheric and Stratospheric Conditions. *J. Geophys. Res*. 107: 4622.

Wexler, A.S, Lurmann, F.W. and Seinfeld, J.H. (1994). Modeling Urban and Regional Aerosols: I. Model Development. *Atmos. Environ*. 28, 531–546.

Wilemski, G. (1984). Composition of the Critical Nucleus in Multicomponent Vapor Nucleation. *J. Chem. Phys*. 80: 1370–1372.

Received for review, November 30, 2011
Accepted, May 22, 2012